J|A|C|S ARTICLES

Published on Web 08/27/2010

pH-Operated Nanopistons on the Surfaces of Mesoporous Silica Nanoparticles

Yan-Li Zhao,[†,‡] Zongxi Li,[†] Sanaz Kabehie,[†] Youssry Y. Botros,[‡,§,||] J. Fraser Stoddart,[*,‡] and Jeffrey I. Zink[*,†]

California NanoSystems Institute and Department of Chemistry and Biochemistry, University of California, Los Angeles, 607 Charles E. Young Drive East, Los Angeles, California 90095, Department of Chemistry, Northwestern University, 2145 Sheridan Road, Evanston, Illinois 60208, Intel Labs, Building RNB-6-61, 2200 Mission College Boulevard, Santa Clara, California 95054, and National Center for Nano Technology Research, King Abdulaziz City for Science and Technology, P.O. Box 6086, Riyadh 11442, Kingdom of Saudi Arabia

Received June 18, 2010; E-mail: stoddart@northwestern.edu; zink@chem.ucla.edu

Abstract: The development of drug delivery systems for the targeted and on-demand release of pharmaceutical products has risen rapidly to become a contemporary challenge in the field of nanobiotechnology. Biocompatible mechanized phosphonate-clothed silica nanoparticles have been designed and fabricated in which the supramolecular machinery, which covers the surfaces of the nanoparticles, behaves like nanopistons, releasing encapsulated guest molecules in a controlled fashion under acidic conditions. The mechanized nanoparticles consist of a monolayer of β-cyclodextrin (β-CD) rings positioned selectively around the orifices of the nanopores of the mesoporous nanoparticles. A rhodamine B/benzidine conjugate was prepared for use as the nanopistons for movement in and out of the cylindrical cavities provided by the β-CD rings on the surfaces of the nanoparticles. Luminescence experiments indicated that the mechanized nanoparticles were able to store small cargo molecules (e.g., 2,6-naphthalenedisulfonic acid disodium) within their nanopores at neutral pH and then release them by passage through the cavities of the β-CD rings as soon as the pH was lowered to $\sim$5. In further investigations, the phosphonate-covered silica nanoparticles were functionalized selectively with the β-CD rings, but on this occasion, the seven linkers attaching the rings to the orifices surrounding the nanopores contained cleavable imine double bonds. The β-CD rings on the surface of the nanoparticles served as gates for the storage of large cargo molecules (e.g., rhodamine B) inside the nanopores of the nanoparticles under neutral conditions. Since imine bonds can be hydrolyzed under acidic conditions, the β-CD rings could be severed from the surface of the nanoparticles when the pH was decreased to 6, releasing the large cargo molecules. The results described here present a significant step toward the development of pH-responsive nanoparticle-based dual drug delivery vehicles that are potentially capable of being interfaced with biological systems.

Introduction

The goal of drug delivery is to administer medicinally active molecules with high specificity to diseased cells in a targeted and controlled manner.[1,2] Recently, mesoporous silica nanoparticles[3] have emerged as an appealing class of drug delivery vehicles for the treatment of diseases[2,4] on account of their sophisticated design and mode of action. There is increasing evidence[5] that the nanoparticles are noncytotoxic and that when they are on the order of 100−200 nm in diameter, they can undergo cellular uptake into acidic lysosomes by means of endocytosis. The nanoparticles have large surface exteriors and porous interiors that can be harnessed as reservoirs for small-molecule drug storage. The size and shape of the nanoparticles can be tuned to maximize cellular uptake, while the dimensions and physical environment of the nanopores inside the nanopar-

[†] University of California, Los Angeles.
[‡] Northwestern University.
[§] Intel Labs.
[||] King Abdulaziz City for Science and Technology.

(1) Schrama, D.; Reisfeld, R. A.; Becker, J. C. *Nat. Rev. Drug Discovery* **2006**, *5*, 147–159.
(2) (a) Davis, M. E.; Chen, Z.; Shin, D. M. *Nat. Rev. Drug Discovery* **2008**, *7*, 771–782. (b) Davis, M. E. *Mol. Pharmaceutics* **2009**, *6*, 659–668.
(3) (a) Torney, F.; Trewyn, B. G.; Lin, V. S.-Y.; Wang, K. *Nat. Nanotechnol.* **2007**, *2*, 295–300. (b) Trewyn, B. G.; Slowing, I. I.; Giri, S.; Chen, H.-T.; Lin, V. S.-Y. *Acc. Chem. Res.* **2007**, *40*, 846–853. (c) Angelos, S.; Johansson, E.; Stoddart, J. F.; Zink, J. I. *Adv. Funct. Mater.* **2007**, *17*, 2261–2271. (d) Park, C.; Oh, K.; Lee, S. C.; Kim, C. *Angew. Chem., Int. Ed.* **2007**, *46*, 1455–1457. (e) Taylor, K. M. L.; Kim, J. S.; Rieter, W. J.; An, H.; Lin, W.; Lin, W. *J. Am. Chem. Soc.* **2008**, *130*, 2154–2155. (f) Park, J.-H.; Gu, L.; von Maltzahn, G.; Ruoslahti, E.; Bhatia, S. N.; Sailor, M. J. *Nat. Mater.* **2009**, *8*, 331–336. (g) Park, C.; Lee, K.; Kim, C. *Angew. Chem., Int. Ed.* **2009**, *48*, 1275–1278. (h) Liong, M.; Angelos, S.; Choi, E.; Patel, K.; Stoddart, J. F.; Zink, J. I. *J. Mater. Chem.* **2009**, *19*, 6251–6257. (i) Aznar, E.; Marcos, M. D.; Martínez-Máñez, R.; Sancenón, F.; Soto, J.; Amorós, P.; Guillem, C. *J. Am. Chem. Soc.* **2009**, *131*, 6833–6843. (j) Liu, J.; Stace-Naughton, A.; Jiang, X.; Brinker, C. J. *J. Am. Chem. Soc.* **2009**, *131*, 1354–1355. (k) Cotí, K. K.; Belowich, M. E.; Liong, M.; Ambrogio, M. W.; Lau, Y. A.; Khatib, H. A.; Zink, J. I.; Khashab, N. M.; Stoddart, J. F. *Nanoscale* **2009**, *1*, 16–39. (l) Carnes, E. C.; Harper, J. C.; Ashley, C. E.; Lopez, D. M.; Brinker, L. M.; Liu, J.; Singh, S.; Brozik, S. M.; Brinker, C. J. *J. Am. Chem. Soc.* **2009**, *131*, 14255–14257.

 10.1021/ja105371u

Scheme 1. Schematic Representation of Nanopistons on Mechanized Phosphonate-Covered Silica Nanoparticles[a]

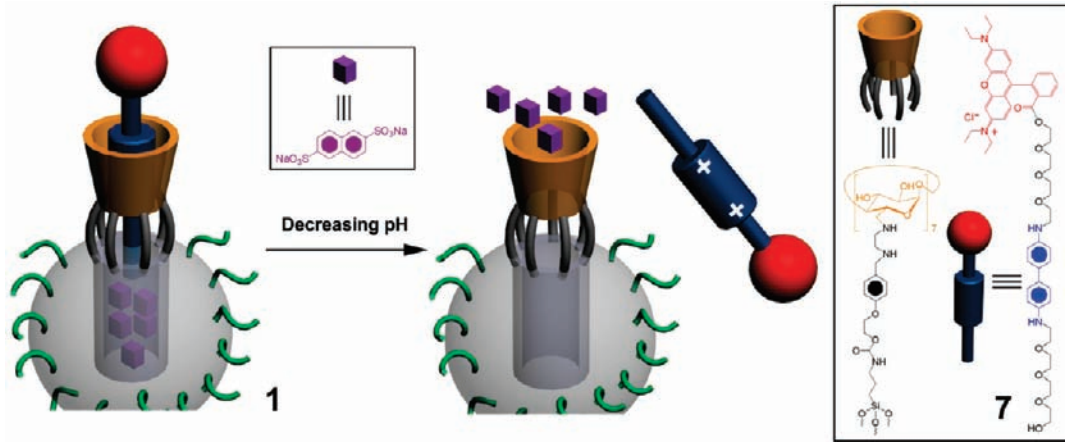

[a] According to the size match of the nanopore and the β-CD ring, the ideal mode is to have one nanopore functionalized with one β-CD ring, as shown in the figure.

ticles can be tailored to store a range of small molecules of different sizes. In particular, the silica nanoparticles can be covered and mechanized with a monolayer of nanovalves[3k] and other artificial molecular[6] and supramolecular[7] machines in order to convert them into smart drug delivery vehicles, that is, mechanized silica nanoparticles (MSNPs) capable of storing and releasing drug molecules on command in response to external stimuli such as pH and/or redox changes, irradiation with light, or the action of enzymes.

In our previous research, the surfaces of the silica nanoparticles were modified[3k] using either switchable [2]pseudorotaxanes or [2]rotaxanes in order to control the loading and release of molecular cargos trapped inside the nanopores. In the early models, the stalks of the [2]pseudorotaxanes and [2]rotaxanes were immobilized on the surfaces of MSNPs, and the movable gates that were employed to control the flow of the cargos from inside the MSNPs included large rings such as (i) the tetracationic cyclophane cyclobis(paraquat-*p*-phenylene) ($CBPQT^{4+}$),[6a−c,7a] (ii) the crown ether dibenzo[24]crown-8 (DB24C8),[7b,c] (iii) cucurbiturils such as cucurbit[6]uril (CB6),[7d,g,h] and (iv) the cyclodextrins (CDs) α-CD and β-CD.[6d,7f,i] In the present work, we have employed phosphonate-covered silica nanoparticles to prepare MSNPs in which β-CD rings are immobilized selectively around the orifices of the nanopores of the nanoparticles and the gates are nanopistons that can be induced to move in or out of the cylindrical cavities provided by the β-CD rings.

The phosphonate-covered silica nanoparticles were prepared from tetraethyl orthosilicate (TEOS) and 3-(trihydroxysilyl)propylmethylphosphonate monosodium (TPMP) using a surfactant-directed self-assembly process[5a] whereby the surfaces of the nanoparticles are covered fully with propyl methylphosphonate units. After the surfactant, cetyltrimethylammonium bromide (CTMA), is removed from the nanopores of the nanoparticles under acidic conditions, the orifices around entrances to the nanopores are exposed for further functionalization. This synthetic strategy has made it possible for us to functionalize only and specifically the exposed areas, namely, the orifices surrounding the entrances to the nanopores, in order to align the nanopores, the β-CD rings, and the nanopistons in a collinear manner. The fabrication process ensures that the β-CD rings are located only at the orifices of the nanopores on the surface of the nanoparticles. A schematic representation of this next generation of MSNPs is shown in Scheme 1. Their design is fashioned according to the following blueprint: β-CD rings persubstituted on their seven C6 positions with kinetically stable linkers serve as the monocylinders that are linked covalently around the orifices of the nanopores of the phosphonate-covered silica nanoparticles. We refer to β-CD rings on the surface of these nanoparticles as heptapuses and the seven linkers connecting the β-CD rings to the nanopores of the nanoparticles as tentacles. Rhodamine B/benzidine conjugates fulfill the role of the nanopistons, which have been designed to move in and out of the nanocylinders provided by the cavities of the β-CD rings[8] in response to changes in pH. In addition, 2,6-naphthalenedisulfonic acid disodium (NDAD) has been employed as the cargo inside the nanopores. Since both rhodamine B and the NDAD cargo have characteristic fluorescent properties, we

(4) Kresge, C. T.; Leonovicz, M. E.; Roth, W. J.; Vartuli, J. C.; Beck, J. S. *Nature* **1992**, *359*, 710–712.
(5) (a) Lu, J.; Liong, M.; Zink, J. I.; Tamanoi, F. *Small* **2007**, *3*, 1341–1346. (b) Liong, M.; Lu, J.; Kovochich, M.; Xia, T.; Ruehm, S. G.; Nel, A. E.; Tamanoi, F.; Zink, J. I. *ACS Nano* **2008**, *2*, 889–896.
(6) (a) Nguyen, T. D.; Tseng, H.-R.; Celestre, P. C.; Flood, A. H.; Liu, Y.; Stoddart, J. F.; Zink, J. I. *Proc. Natl. Acad. Sci. U.S.A.* **2005**, *102*, 10029–10034. (b) Nguyen, T. D.; Leung, K. C.-F.; Liong, M.; Liu, Y.; Stoddart, J. F.; Zink, J. I. *Adv. Funct. Mater.* **2007**, *17*, 2101–2110. (c) Nguyen, T. D.; Liu, Y.; Saha, S.; Leung, K. C.-F.; Stoddart, J. F.; Zink, J. I. *J. Am. Chem. Soc.* **2007**, *129*, 626–634. (d) Patel, K.; Angelos, S.; Dichtel, W. R.; Coskun, A.; Yang, Y.-W.; Zink, J. I.; Stoddart, J. F. *J. Am. Chem. Soc.* **2008**, *130*, 2382–2383. (e) Lu, J.; Choi, E.; Tamanoi, F.; Zink, J. I. *Small* **2008**, *4*, 421–426. (f) Liong, M.; France, B.; Bradley, K. A.; Zink, J. I. *Adv. Mater.* **2009**, *21*, 1684–1689. (g) Vivero-Escoto, J. L.; Slowing, I. I.; Wu, C.-W.; Lin, V. S.-Y. *J. Am. Chem. Soc.* **2009**, *131*, 3462–3463.
(7) (a) Hernandez, R.; Tseng, H.-R.; Wong, J. W.; Stoddart, J. F.; Zink, J. I. *J. Am. Chem. Soc.* **2004**, *126*, 3370–3371. (b) Nguyen, T. D.; Leung, K. C.-F.; Liong, M.; Pentecost, C. D.; Stoddart, J. F.; Zink, J. I. *Org. Lett.* **2006**, *8*, 3363–3366. (c) Leung, K. C.-F.; Nguyen, T. D.; Stoddart, J. F.; Zink, J. I. *Chem. Mater.* **2006**, *18*, 5919–5928. (d) Angelos, S.; Yang, Y.-W.; Patel, K.; Stoddart, J. F.; Zink, J. I. *Angew. Chem., Int. Ed.* **2008**, *47*, 2222–2226. (e) Liu, R.; Zhao, X.; Wu, T.; Feng, P. *J. Am. Chem. Soc.* **2008**, *130*, 14418–14419. (f) Ferris, D. P.; Zhao, Y.-L.; Khashab, N. M.; Khatib, H. A.; Stoddart, J. F.; Zink, J. I. *J. Am. Chem. Soc.* **2009**, *131*, 1686–1688. (g) Angelos, S.; Yang, Y.-W.; Khashab, N. M.; Stoddart, J. F.; Zink, J. I. *J. Am. Chem. Soc.* **2009**, *131*, 11344–11346. (h) Angelos, S.; Khashab, N. M.; Yang, Y.-W.; Trabolsi, A.; Khatib, H. A.; Stoddart, J. F.; Zink, J. I. *J. Am. Chem. Soc.* **2009**, *131*, 12912–12914. (i) Du, L.; Liao, S.; Khatib, H. A.; Stoddart, J. F.; Zink, J. I. *J. Am. Chem. Soc.* **2009**, *131*, 15136–15142.
(8) (a) Tian, H.; Wang, Q.-C. *Chem. Soc. Rev.* **2006**, *35*, 361–374. (b) Frampton, M. J.; Anderson, H. L. *Angew. Chem., Int. Ed.* **2007**, *46*, 1028–1064.

Scheme 2. Synthetic Procedure for the Mechanized Silica Nanoparticle-Based Nanopistons **1**

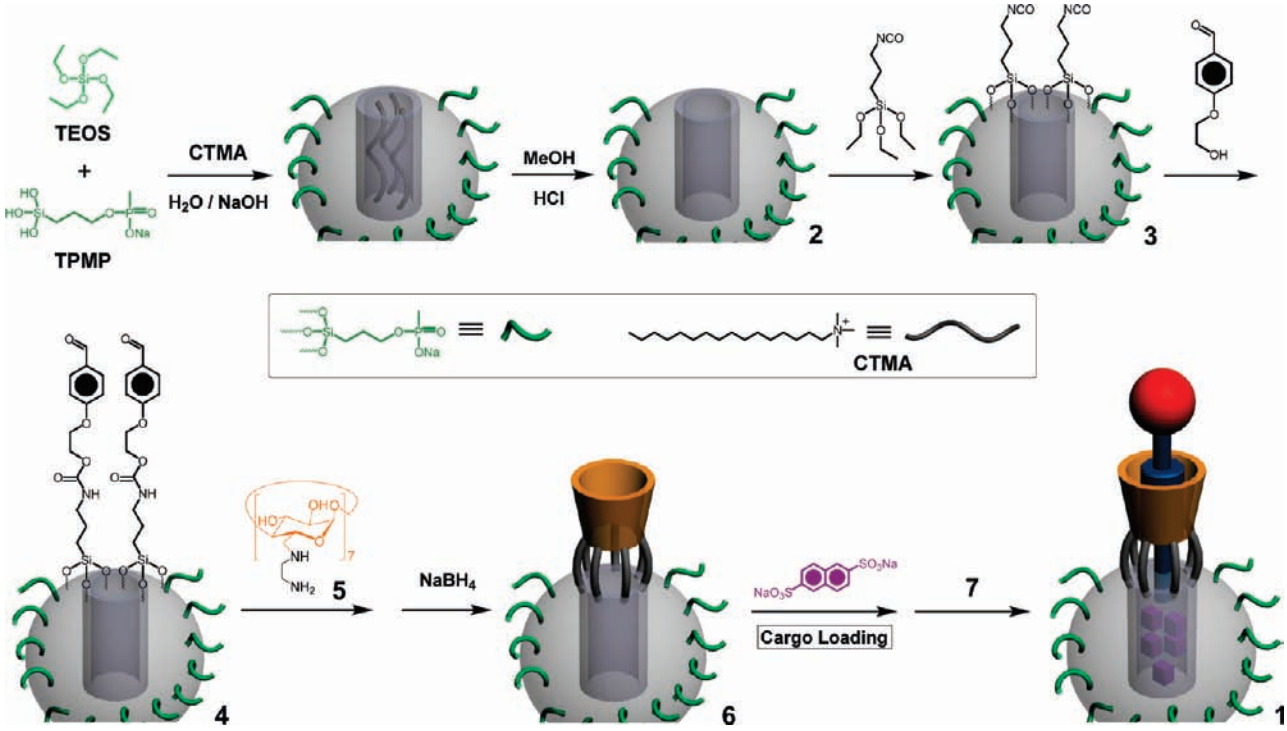

can monitor the operation of the nanopistons by following the changes in their luminescent properties.

Results and Discussion

The synthetic procedure for the preparation of the mechanized silica nanoparticle-based nanopistons **1** is shown in Scheme 2. 3-Isocyanatopropyltriethoxysilane (3-ICPES)-functionalized nanoparticles **3** were prepared from phosphonate silica nanoparticles **2** and 3-ICPES in PhMe. These nanoparticles **3** were treated with 4-(2-hydroxyethoxy)benzaldehyde to afford the formyl-functionalized nanoparticles **4**, which were reacted with the diamino-β-CD derivative **5** by means of a series of Schiff base reactions. After the C═N double bonds were reduced to C−N single bonds by addition of sodium borohydride, the β-CD-capped nanoparticles **6** were isolated. The MSNP-based nanopistons **1** were finally obtained after the capped nanoparticles **6** were loaded with the NDAD cargo and the rhodamine B/benzidine plug **7**, which had been prepared from rhodamine B and the benzidine oligoethylene glycol derivative by means of a DCC coupling reaction (Scheme 3). The β-CD-capped phosphonate silica nanoparticles **6** were characterized by transmission electron microscopy (TEM), powder X-ray diffraction (XRD), and ^{13}C and ^{29}Si cross-polarization magic-angle-spinning (CP−MAS) solid-state NMR spectroscopy.

The size and shape of the phosphonate silica nanoparticles **2** were evaluated (Figure 1) using TEM. The nanoparticles are roughly spherical in shape and ∼100 nm in diameter. They possess perfect hexagonal nanopore arrays with an average nanopore diameter of 2.2 nm. The nanoparticles also show XRD patterns typical of MCM-41-type hexagonal mesoporous silica.[4] An interplanar spacing (d_{100}) of ∼3.8 nm was calculated from these patterns. It appears that when the nanoparticles are functionalized with the β-CD rings, the shape of the nanoparticles experiences no obvious changes, at least as judged by TEM and XRD, indicating that the β-CD-capped MSNPs retain the characteristics of mesoporous silica nanoparticles.

CP−MAS solid-state NMR experiments provide direct evidence of the formation of the β-CD-capped nanoparticles. Examination of the ^{13}C CP−MAS solid-state NMR spectrum of the capped nanoparticles **6** (Figure 2a) shows that (i) the signals resonating around 22 ppm can be attributed to the characteristic peaks of aliphatic carbons *l* and *m* on the linker

Scheme 3. Synthetic Procedure for the Rhodamine B/Benzidine Plug **7**

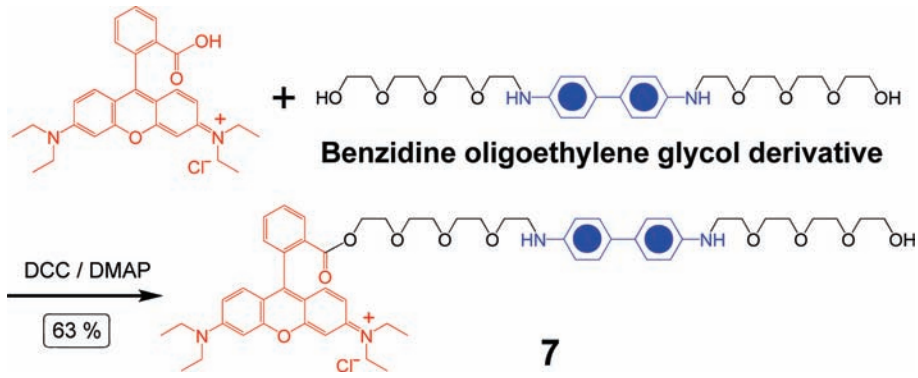

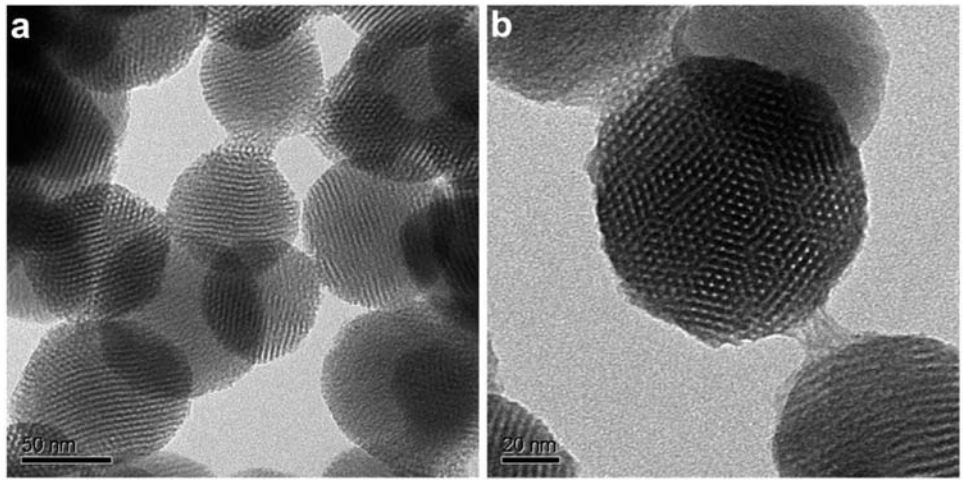

Figure 1. TEM images of the phosphonate-covered silica nanoparticles **2** at (a) low and (b) high resolution.

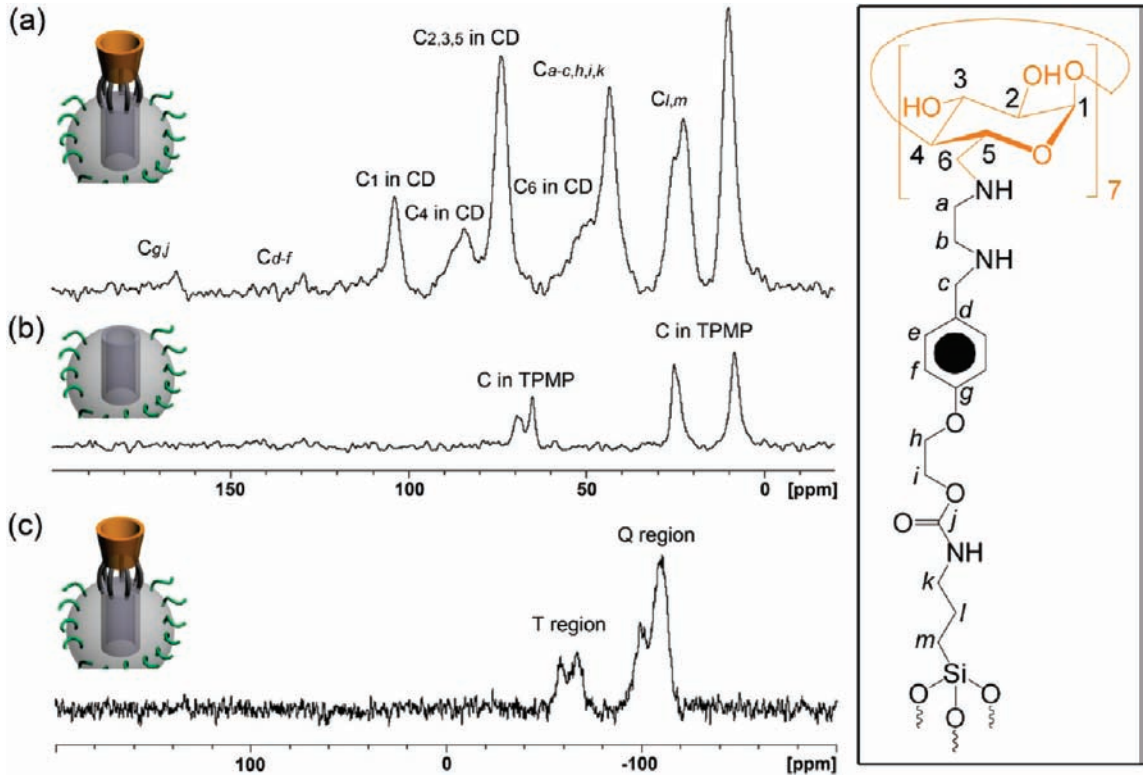

Figure 2. ^{13}C and ^{29}Si CP−MAS solid-state NMR spectra. (a) ^{13}C CP−MAS solid-state NMR spectrum of the β-CD-capped nanoparticles **6**. (b) ^{13}C CP−MAS solid-state NMR spectrum of the phosphonate-covered silica nanoparticles **2**. (c) ^{29}Si CP−MAS solid-state NMR spectrum of the capped nanoparticles **6**. The carbon nuclei of the β-CD ring and the linker are defined alongside the structural formula.

between the β-CD ring and the phosphonate silica nanoparticle; (ii) the signals resonating around 45 ppm can be assigned to the characteristic peaks of carbons *a*, *b*, *c*, *h*, *i*, and *k* on the linker; (iii) the signals resonating around 50, 73, 84, and 104 ppm can be attributed to the characteristic carbon peaks of C_6, $C_{2/3/5}$, C_4, and C_1 on the β-CD skeleton, respectively;[9] (iv) the signals resonating around 130 ppm can be assigned to the characteristic peaks of aromatic carbons *d*, *e*, and *f* of the phenyl groups; and (v) the signals resonating around 165 ppm can be attributed to the characteristic peaks of carbons *g* and *j*. From an examination of the ^{13}C CP−MAS solid-state NMR spectrum of the nanoparticles **2** (Figure 2b), we know that the carbon nuclei of the TPMP units also contribute to the signals resonating around 9, 22, and 65 ppm. The ^{29}Si CP−MAS solid-state NMR spectrum (Figure 2c) of the nanoparticles **6** shows two silicon peaks around −60 and −105 ppm, corresponding[10] to the functionalized silica (T region) and bulk silica (Q region), respectively. Although the silicon nuclei in the nanoparticles **2** also give rise to two peaks attributable to the phosphonate silica (T region) and bulk silica (Q region), the peak around −60 ppm in the phosphonate-covered silica nanoparticles **2** is of relatively low intensity in comparison with that observed for the capped

(9) Gidley, M. J.; Bociek, S. M. *J. Am. Chem. Soc.* **1988**, *110*, 3820–3829.

(10) Peng, C.; Zhang, H.; Yu, J.; Meng, Q.; Fu, L.; Li, H.; Sun, L.; Guo, X. *J. Phys. Chem. B* **2005**, *109*, 15278–15287.

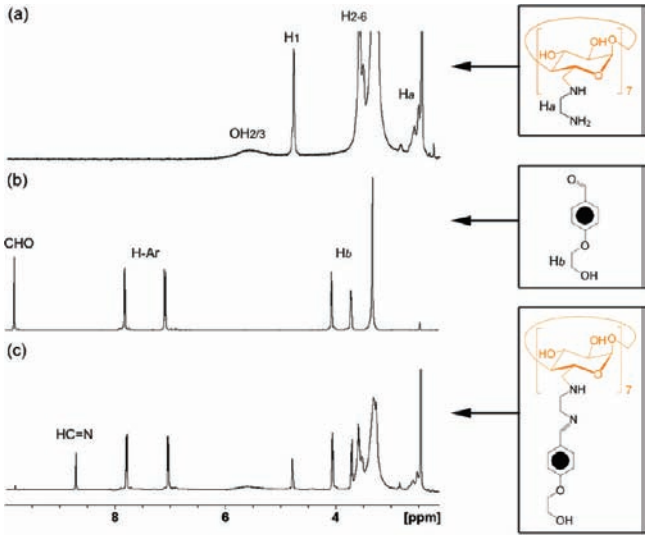

Figure 3. (a) ^{1}H NMR spectrum (500 MHz) of diamino-β-CD derivative **5** (1.0×10^{-3} mol L^{-1}) in CD_3SOCD_3 at 25 °C. (b) ^{1}H NMR spectrum (500 MHz) of 4-(2-hydroxyethoxy)benzaldehyde (7.0×10^{-3} mol L^{-1}) in CD_3SOCD_3 at 25 °C. (c) ^{1}H NMR spectrum (500 MHz) after mixing diamino-β-CD derivative **5** (1.0×10^{-3} mol L^{-1}) and 4-(2-hydroxyethoxy)-benzaldehyde (7.0×10^{-3} mol L^{-1}) in CD_3SOCD_3 at 25 °C.

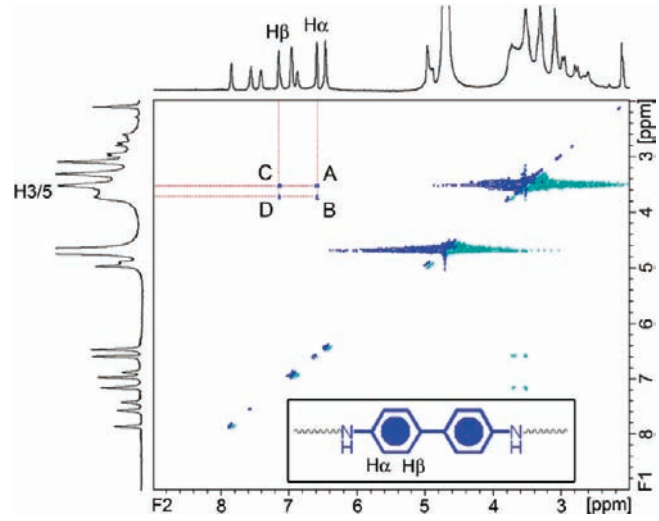

Figure 4. ^{1}H ROESY NMR spectrum (600 MHz) of diamino-β-CD derivative **5** (8.5×10^{-4} mol L^{-1}) with the plug **7** (8.5×10^{-4} mol L^{-1}) in D_2O at 25 °C with a mixing time of 250 ms.

nanoparticles **6**. The Schiff base reaction between diamino-β-CD derivative **5** and the formyl group was also monitored by ^{1}H NMR spectroscopy (Figure 3). Mixing **5** (1.0×10^{-3} mol L^{-1}) and 4-(2-hydroxyethoxy)benzaldehyde (7.0×10^{-3} mol L^{-1}) in CD_3SOCD_3 resulted in the appearance of a new peak resonating at 8.73 ppm in the ^{1}H NMR spectrum, indicating the formation of the imine double bonds. These NMR spectroscopic experiments demonstrated that the synthetic procedure for the preparation of the β-CD-capped nanoparticles was successful.

In order to determine the binding affinity of the β-CD ring with the benzidine unit on the plug **7**, isothermal calorimetry (ITC) titration experiments were performed in an aqueous buffer solution at 25 °C. In view of the fact that the pK_a of the benzidine unit[11] is ~4.8, we selected the β-CD ring and the plug as a model system to investigate the binding affinity in H_2O under different pH conditions. The formation constant (K_f) for the complex of the β-CD ring with the plug is 8605 ± 85 M^{-1} at pH 7.0, whereas it is less than 70 at pH 2.0. It follows that the benzidine unit of the plug binds to the inner cavity of the β-CD ring on the nanoparticles under neutral conditions. When the pH is decreased, the positively charged benzidine unit dissociates from the cavity, resulting in release of the cargo molecules in the nanopores. The value of K_f for the complex of the β-CD ring with the NDAD cargo molecule[12] is 410 ± 20 M^{-1} at pH 5.5. The cargo molecule does not bind to the β-CD ring in the presence of the plug.

The fact that plug **7** can be inserted into the cavity of diamino-β-CD derivative **5** was confirmed by an ^{1}H ROESY NMR experiment. The protons at the 3 and 5 positions on the β-CD ring point toward the inside of the cavity. Identification of cross-peaks between the 3 and 5 protons and the protons of the guest molecules in the ROESY spectrum is thus indicative of the fact that the guest molecules are included inside the cavity of the β-CD ring.[13] An ^{1}H ROESY NMR experiment on the complex formed between **5** (8.5×10^{-4} mol L^{-1}) and **7** (8.5×10^{-4} mol L^{-1}) was performed in D_2O at 25 °C. NOE cross-peaks between (i) the H_α protons of the benzidine unit in the plug and the $H_{3/5}$ protons on the inside of the β-CD ring (peaks A and B) and (ii) the benzidine H_β protons and the $H_{3/5}$ protons on the β-CD ring (peaks C and D) were observed (Figure 4) in the ^{1}H ROESY spectrum. However, no NOE crosspeaks between the $H_{3/5}$ protons of diamino-β-CD derivative **5** and the protons of the rhodamine B unit on the plug **7** could be identified. These observations indicate that (i) the benzidine unit within the plug is included inside the hydrophobic cavity of the β-CD ring, as illustrated in Scheme 1, and (ii) the rhodamine B unit does not enter into any interactions with the hydrophobic cavity of the β-CD ring.

In order to obtain further evidence to support the belief that the vast majority of the β-CD rings are linked around the orifices of the nanopores on the mesoporous silica nanoparticles, we performed calculations. The hydroxyl (OH) coverage of the amorphous silicates was determined using a deuterium exchange method reported in the literature.[14] Using this method, we discovered that the average OH coverage for the silica nanoparticles and silica gels was 4.9 hydroxyl groups/nm^2. This value corresponds closely to the value obtained when the amorphous silica surfaces are represented by the ⟨111⟩ octahedral face of cristobalite, which has a density and refractive index similar to those of amorphous silica.[15] Calculations based on the model of cristobalite with the ⟨111⟩ octahedral face[16] strongly support the proposed mode of functionalization of the nanoparticles described in Scheme 1, i.e., one nanopore functionalized with one β-CD ring through its seven C6 positions. In addition, we also calculated[17] the theoretical number of nanopores associated with each nanoparticle. The average number of nanopores on the surface of a representative average-sized nanoparticle was 2260.

(11) You, Z.; Brezzell, M. D.; Das, S. K.; Espadas-Torre, M. C.; Hooberman, B. H.; Sinsheimer, J. E. *Mutat. Res.* **1993**, *319*, 19–30.
(12) Hamai, S.; Ishikawa, S. *Spectrochim. Acta, Part A* **2001**, *57*, 1–8.
(13) Schneider, H.-J.; Hacket, F.; Rüdiger, V. *Chem. Rev.* **1998**, *98*, 1755–1786.
(14) (a) Zhuravlev, L. T. *Langmuir* **1987**, *3*, 316–318. (b) Armistead, C. G.; Tyler, A. J.; Hambleton, F. H.; Mitchell, S. A.; Hockey, J. A. *J. Phys. Chem.* **1969**, *73*, 3947–3953.
(15) Brinker, C. J.; Scherer, G. W. *Sol−Gel Science*; Academic Press: New York, 1990.

On the basis of the large K_f value ($8605 \pm 85\ M^{-1}$) for the complex between the β-CD ring and the plug, the extent to which the plugs occupy the β-CD heptapuses on the nanoparticles under neutral conditions could be estimated. Despite the fact that the plugs bind with the β-CD rings on the surfaces of the mechanized nanoparticles at the interface of the aqueous solution and the β-CD monolayer, we assumed that the sites of host−guest binding between the plugs and the β-CD rings are equivalent and independent.[18] Thus, the formation constant for complexation of the plug to a single β-CD ring on the surface of a mechanized nanoparticle at the interface was assumed to be comparable to the K_f value for this host−guest pair in aqueous solution. In the particular procedure for the preparation of the silica nanoparticle-based nanopistons, the initial concentrations of the β-CD rings and the plugs were calculated to be 2.46×10^{-5} and 2.0×10^{-3} M, respectively; from these, we computed the concentration of the complex to be 2.32×10^{-5} M.[19] Therefore, the percentage of plugs filling the β-CD heptapuses on the nanoparticles at the concentrations in question was $100\% \times (2.32 \times 10^{-5}\ M)/(2.46 \times 10^{-5}\ M) = 94\%$. In view of this high coverage, it is hardly surprising that the silica nanoparticle-based nanopistons do not exhibit any serious leakage under neutral conditions.

The operation of the MSNP-based nanopistons **1** was monitored in aqueous solution by fluorescence spectroscopy. A sample of the NDAD-loaded nanoparticles (5 mg) was placed in the corner of a cuvette, and distilled H_2O (5 mL, pH 7) was added very carefully to the cuvette to avoid disturbing the nanoparticles. A laser probe beam directed into the solution was used to excite the released cargo molecules. The emission intensities of these molecules were collected as a function of time and used to generate a release profile. The pH of the solution was adjusted to the desired value by the addition of HCl solution (0.1 M). The percentage of the cargo released was calculated using absorbance spectroscopy to enable quantitative comparison of the release efficiency. Since there are two fluorescent units in the system, namely, the rhodamine B unit on **7** and the NDAD cargo, we monitored the release profiles of the nanoparticles using two laser sources, one operating at 448 nm[20] to monitor the rhodamine B unit and the other at 377 nm to monitor the NDAD cargo. Figure 5a,b shows the release profiles of the rhodamine B unit and NDAD cargo, respectively, from the MSNP-based nanopistons **1**. The flat baselines (black curves) indicate that both the rhodamine B unit and the NDAD cargo did not leak from the nanopistons **1** under neutral conditions. The emission intensity of the solution before any pH-triggered release was monitored for over 40 min. The pH value of the system was then decreased from 7 to 4 by the addition of 0.1 M HCl. As the protonated plugs **7** left the cavities of the β-CD rings on the nanoparticles, the NDAD cargo was released from the nanopores of the nanoparticles, and we monitored the fluorescence changes of the solution in order to evaluate the cargo storage and release abilities of the MSNPs in response to the pH changes. After the pH was lowered, the emission intensities of both the rhodamine B unit and the NDAD cargo in solution increased immediately, confirming that the positively charged plug **7** was no longer blocking the β-CD ring on the nanopores of the nanoparticle and in turn that the NDAD cargo in the nanopores was released into the solution. In a control experiment, NDAD-loaded nanoparticles **6** without

(16) Using the model of cristobalite with the ⟨111⟩ octahedral face, we can calculate that the Si−O bond length (d_{Si-O}) is 1.626 Å, the O−O bond length (d_{O-O}) is 2.656 Å [$d_{O-O} = 2d_{Si-O} \sin[\angle(O-Si-O)/2] = (2)(1.626\ Å) \sin(109.5°/2)$], and the Si−Si bond length (d_{Si-Si}) is 5.312 Å ($d_{Si-Si} = 2d_{O-O}$). Therefore, the distance between two OH groups on the surface is 5.312 Å. Since the TEM images showed that the average diameter (d) of the nanopores is 2.2 nm, the average perimeter (p) of the nanopores is 69.1 Å [$p = \pi d = \pi(2.2\ nm)$], and in turn, the number of OH groups around one nanopore (N_{OH}) on the silica surfaces is 13 [$N_{OH} = p/d_{Si-Si} = (69.1\ Å)/(5.312\ Å)$]. Since the diamino-$\beta$-CD derivative **5** has seven tentacles at its C6 positions and the attachment of one tentacle spatially requires a distance between two OH groups on the nanopore perimeter, the number of tentacles (N_t) that can be attached around one nanopore is ~7 (≈13/2), a number that matches rather well with the number of C6 positions on a β-CD ring. Thus, the calculations support the proposed mode of functionalization of the nanoparticles described in Scheme 1, i.e., one nanopore functionalized by and large with one β-CD ring through its seven C6 positions.

(17) On the basis of the surface area of one silica nanosphere [$A_{ns} = 4\pi(50\ nm)^2 = 31416\ nm^2$], the area of one repeating unit ($A_u = 13.9\ nm^2$) obtained from the XRD lattice distance, and the area of one nanopore [$A_{np} = \pi(1.1\ nm)^2 = 3.8\ nm^2$] obtained from the TEM experiments, we can calculate that (i) the volume of one solid nanosphere (V_s) is $5.24 \times 10^5\ nm^3$ [$V_s = {}^4/_3\pi(50\ nm)^3$] and (ii) the volume of one nanoparticle (V_{np}) is $3.81 \times 10^5\ nm^3$ [$V_{np} = V_s(1 - A_{np}/A_u) = (5.24 \times 10^5\ nm^3)(1 - 3.8\ nm^2/13.9\ nm^2)$]. As the density ($D$) of amorphous silicate is 2.0 g/cm^3, the mass of one nanoparticle (m_{np}) would be 7.62×10^{-16} g [$m_{np} = V_{np}D = (3.81 \times 10^5\ nm^3)(2.0 \times 10^{-21}\ g/nm^3)$]. Finally, the number of nanopores (N_{np}) on one nanoparticle is ~2260 ($N_{np} = A_{ns}/A_u = 31416\ nm^2/13.9\ nm^2$).

(18) (a) Mulder, A.; Auletta, T.; Sartori, A.; Ciotto, S. D.; Casnati, A.; Ungaro, R.; Huskens, J.; Reinhoudt, D. N. *J. Am. Chem. Soc.* **2004**, *126*, 6627–6636. (b) Corbellini, F.; Mulder, A.; Sartori, A.; Ludden, M. J. W.; Casnati, A.; Ungaro, R.; Huskens, J.; Crego-Calama, M.; Reinhoudt, D. N. *J. Am. Chem. Soc.* **2004**, *126*, 17050–17058. (c) Crespo-Biel, O.; Lim, C. W.; Ravoo, B. J.; Reinhoudt, D. N.; Huskens, J. *J. Am. Chem. Soc.* **2006**, *128*, 17024–17032. (d) Ludden, M. J. W.; Li, X.; Greve, J.; van Amerongen, A.; Escalante, M.; Subramaniam, V.; Reinhoudt, D. N.; Huskens, J. *J. Am. Chem. Soc.* **2008**, *130*, 6964–6973.

(19) The calculations assume that the phosphonate-covered silica nanoparticles are fully attached to the β-CD heptapuses with one β-CD ring position as an extension over each nanopore (somewhat like a porch outside the front door of a house). During the preparation of the silica nanoparticle-based nanopistons (see the Experimental Section), 50 mg of the phosphonate-covered silica nanoparticles and a solution volume of 10 mL were used. Thus, the concentration of the β-CD ring is [β-CD]$_0 = 2.46 \times 10^{-5}$ M [(total weight of the nanoparticle/weight of individual nanoparticle/Avogadro constant) × (number of β-CD rings on one nanoparticle)/(volume of solution) = [(0.05 g)/(7.62×10^{-16} g)/($6.02 \times 10^{23}\ mol^{-1}$) × (2260)/(0.01 L)], and the concentration of the plug is [plug]$_0 = 2.0 \times 10^{-3}$ M (0.02 mmol/0.01 L). For the complex of a β-CD ring with a plug, K_f is defined as

$$K_f = \frac{[\text{complex}]_{eq}}{[\text{plug}]_{eq}[\beta\text{-CD}]_{eq}}$$

where "eq" subscripts denote equilibrium concentrations. Using the measured K_f value ($8605 \pm 85\ M^{-1}$) in this equation gives

$$\begin{aligned} 8605\ M^{-1} &= \frac{[\text{complex}]_{eq}}{[\text{plug}]_{eq}[\beta\text{-CD}]_{eq}} \\ &= [\text{complex}]_{eq}/\{([\text{plug}]_0 - [\text{complex}]_{eq}) \times \\ &\qquad ([\beta\text{-CD}]_0 - [\text{complex}]_{eq})\} \\ &= [\text{complex}]_{eq}/\{(2.0 \times 10^{-3}\ M - [\text{complex}]_{eq}) \times \\ &\qquad (2.46 \times 10^{-5}\ M - [\text{complex}]_{eq})\} \end{aligned}$$

which can be solved to obtain a concentration of 2.32×10^{-5} M for the complex.

(20) Although the excitation beam with a longer wavelength has lower energy, it can excite a strong enough emission by rhodamine B. A lower-energy beam has less chance of causing damage to the nanoparticles as well as being less likely to induce a photobleaching effect. We therefore employed the laser source at 448 nm with a lower energy that is closer to the emission wavelength of rhodamine B during the fluorescence experiments.

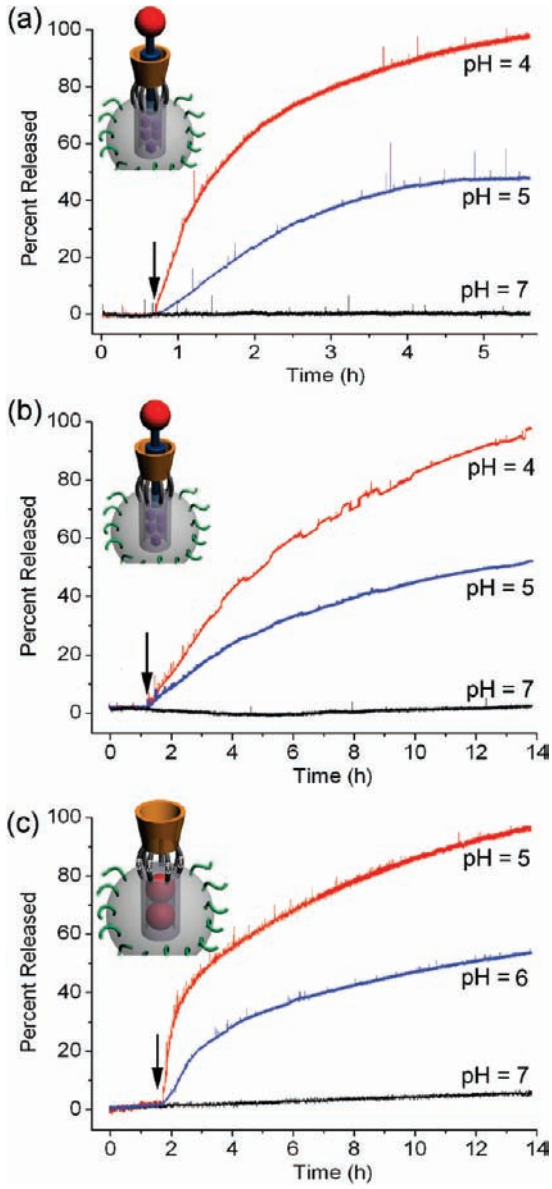

Figure 5. Release profiles of the MSNPs under pH control. (a) Release profile for MSNP-based nanopistons **1** while monitoring the 565 nm emission of the rhodamine B unit on the plug **7**. (b) Release profile for **1** while monitoring the NDAD cargo emission at 415 nm. (c) Release profile of MSNPs **8** while monitoring the rhodamine B cargo emission at 565 nm. Note the change in time scales between panel (a) and panels (b) and (c).

plug **7** showed a sustained release profile when the loaded nanoparticles were not washed. However, when the NDAD-loaded nanoparticles were washed thoroughly, no fluorescence changes were observed even after the pH of the solution was lowered. The reason for this difference lies in the fact that the NDAD cargo molecules escaped through the unblocked β-CD rings on the nanopores of the nanoparticles during the washing process.

The release profiles (Figure 5a,b) demonstrate well the fact that the nanopistons can contain cargo molecules at neutral pH but release them when the pH is decreased to a particular level. The rate of the release of the nanopistons depends directly on the pH used for activation, with the highest release rate occurring at the most acidic pH value. In the case where we monitored the rhodamine B unit (Figure 5a), when the pH was adjusted to 4, 100% of the plug molecules were removed from the cavities of the β-CD rings on the nanoparticles after 5.6 h. However, when the pH was adjusted to 5, only 49% of the plug molecules were removed in the same amount of time. The observed pH-dependent release rate is consistent with the proposed mechanism for the operation of the nanopistons, i.e., the degree of the plug removal depends on the rate of protonation of the benzidine nitrogen atoms on the plug **7**, and this process occurs more rapidly at more acidic pH. UV−vis absorption spectroscopy was used to calculate that ~0.2 μmol of plug (~4.0 wt %) was removed from the cavities of the β-CD rings on the nanoparticles (5 mg in 5 mL aqueous solution) after 5.6 h at pH 4.

A comparison of the release profile for the NDAD cargo (Figure 5b) with that for the rhodamine B units (Figure 5a) reveals a difference in the pH sensitivity. When a pH of 4 was used to activate the nanopistons, 58% of the maximum cargo release was obtained after 5.6 h and 100% release was achieved after 13.9 h. When the pH was 5, 31 and 52% of the maximum NDAD cargo was released after 5.6 and 13.9 h, respectively. The lower release efficiency of the NDAD cargo than of the plug **7** at the same pH value indicates that (a) after the plug departs from the cavity of the β-CD ring on the nanoparticles, the NDAD cargo is released into the solution, and (b) the plug is more readily removed on account of the electrostatic repulsion between the positively charged plug and the cavity of the β-CD ring. UV−vis absorption spectroscopy was used to calculate that ~0.8 μmol of the NDAD cargo was released from the nanopores of the nanoparticles (5 mg in 5 mL aqueous solution) at pH 4 after 13.9 h. This release capacity corresponds to a maximum of ~5.3 wt %.

In another control experiment, we prepared nanoparticles **8** (Figure 6) from diamino-β-CD derivative **5** and the formyl-functionalized nanoparticles **4** in the presence of rhodamine B cargo using the Schiff base reaction. The rhodamine B molecule is larger in size than the cavity of the β-CD ring, so the rhodamine B molecules are blocked inside the nanopores of the nanoparticles by the β-CD rings. Since the C═N double bonds formed between diamino-β-CD derivative **5** and the formyl groups can be broken under acidic conditions, the β-CD rings can be removed from the surfaces of the nanoparticles very easily, resulting in the release of the rhodamine B cargo from the nanopores of the nanoparticles. In the release profile of this system (Figure 5c), the flat baseline (black curve) indicates that the rhodamine B cargo did not leak from the nanoparticles **8** under neutral conditions. When the pH was decreased to 6, however, 37 and 54% of the maximum cargo was released after 5.6 and 13.9 h, respectively. When pH 5 was employed to activate the nanoparticle, 66 and 100% of the maximum cargo was released after 5.6 and 13.9 h, respectively. On the basis of UV−vis absorption spectroscopy, we calculated that ~0.5 μmol of the rhodamine B cargo was released from the nanopores of the nanoparticles (5 mg in 5 mL aqueous solution) at pH 5 after 13.9 h, corresponding to a maximum of ~4.8 wt %.

Conclusion

On the basis of the tenets of supramolecular chemistry[21] and mechanostereochemistry,[22] we have described the nanoscale

(21) Stoddart, J. F. *Nat. Chem.* **2009**, *1*, 14–15.
(22) Olson, M. A.; Botros, Y. Y.; Stoddart, J. F. *Pure Appl. Chem.* **2010**, *82*, 1569–1574.

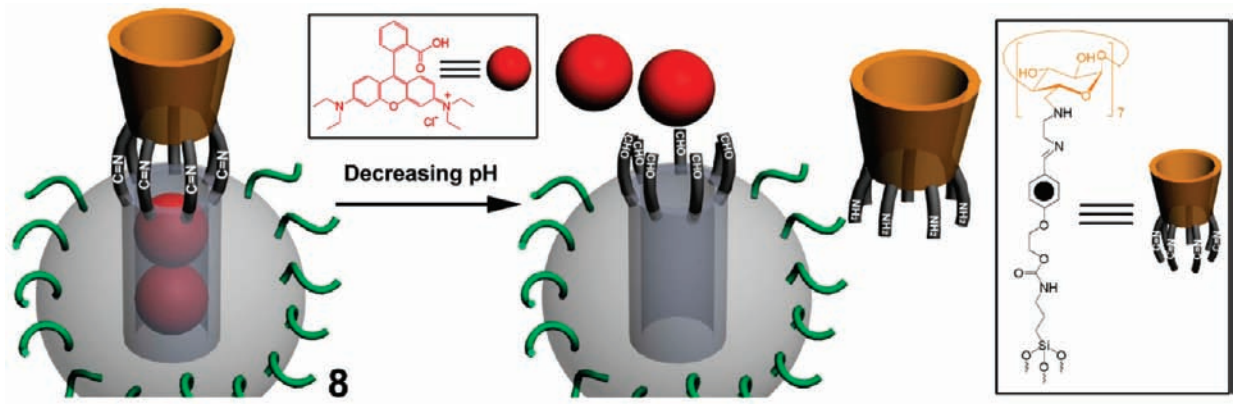

Figure 6. Schematic representation of the phosphonate-covered MSNPs **8**, which were prepared from diamino-β-CD derivative **5** and the formyl-functionalized nanoparticles **4** in the presence of rhodamine B cargo by means of the Schiff base reaction.

fabrication and pH-responsive operation of phosphonate-covered mesoporous silica nanoparticle-based nanopistons. β-CD rings were attached covalently with structural precision around the orifices of the nanopores of these protected nanoparticles, creating an inorganic−organic material that constitutes an integrated system. The introduction of the β-CD rings around the orifices of the nanopores on the spherical surfaces of the nanoparticles affords much greater stereoelectronic control over the entrapment and release of small-molecule cargos than we have achieved previously in our design and fabrication of mechanized silica nanoparticles. The next generation of this particular class of nanoparticles allows for much more delicately controlled monolayers of nanopistons covering their surfaces. The β-CD rings not only constitute a chemical modification of mechanized mesoporous silica nanoparticles but also impose stereoelectronic control upon the orifices of the nanopores at the surfaces of the nanoparticles. As far as the nanopistons on the surfaces of the mechanized silica nanoparticles are concerned, the rhodamine B/benzidine plug can slide in and out of the cylindrical cavities provided by the β-CD rings on the surfaces of the nanoparticles in order to control the trapping and release of the cargo molecules in response to pH changes. A few carefully chosen spectroscopic techniques have demonstrated that the nanopistons are able to incorporate cargo molecules inside the nanopores of the nanoparticles under neutral pH conditions but release them when the pH is lowered just a little. Fluorescent molecules were chosen as the cargos in order to establish a proof-of-principle operation of nanopiston-operated mesoporous silica nanoparticles.

The advantages of the mesoporous silica nanoparticle-based nanopiston system can be summarized as follows: (i) Since the fabrication process of the nanopiston system ensures that the β-CD rings are located only at the orifices of the nanopores on the surface of the nanoparticles, the β-CD rings become essentially an extension of the orifices of the nanopores. Thus, the orifices of the nanopores are regulated by the uniform diameter of the β-CD rings. (ii) Since the β-CD rings on the surfaces of the nanoparticles can form complexes with a series of guest molecules in their hydrophobic cavities, molecular plugs can be designed and synthesized to respond to stimuli that trigger pH-, light-, or redox-operated drug delivery. (iii) Since both the matching molecular plugs and the β-CD rings are removable with changes in pH, the hybrid nanoparticles can in principle be fabricated to display a dual-cargo release mechanism wherein the plugs and the β-CD rings retain small and large drug molecules, respectively. Moreover, the mechanized nanoparticles should release only the small drug molecules when the plugs are removed from the cavities of the β-CD rings at, say, one particular pH, while they can subsequently release the large drug molecules when the β-CD rings on the surfaces of the nanoparticles are severed at some other pH. (iv) Finally, since the plugs can be readily functionalized with targeting antenna, it should be possible to instruct the nanoparticles to hunt down certain diseased cells prior to delivering a specific drug selectively to these cells. Further investigations will employ this integrated nanosystem to carry anticancer drugs and perform pH-responsive drug release in vivo. This ability to fine-tune mesoporous silica nanoparticles for responsive drug delivery enhances their versatility enormously and could one day find application in the treatment of human cancer cells, in view of the fact that their lysosomal pH levels are somewhat lower that the pH levels found in healthy human cells.

Experimental Section

Materials. All of the reagents, including benzidine, CTMA, β-CD, ethylenediamine, 3-ICPES, NDAD, TEOS, TPMP, and rhodamine B, were obtained commercially and used without further purification. The benzidine oligoethylene glycol derivative,[23] 4-(2-hydroxyethoxy)benzaldehyde,[24] and per-6-iodo-β-CD[25] were all prepared according to literature procedures.

General Methods. β-CD derivatives were purified on a Sephadex G-25 column with H_2O as the eluent. Deuterated solvents (Cambridge Isotope Laboratories) for NMR spectroscopic analyses were used as received. Solution NMR spectra were recorded on a Bruker Avance 500 or 600 spectrometer at 25 °C. Chemical shifts were reported in parts per million (ppm) downfield from the Me_4Si resonance, which was used as the internal standard when ^1H NMR spectra were recorded. All of the solid-state NMR spectra were acquired on dry powder samples and were recorded at room temperature on a Bruker DSX 300 MHz spectrometer equipped with a 4 mm broadband double air-bearing MAS probe head using 4 mm ZrO_2 rotors with Kel-F caps. A sample rotation speed of 10 kHz was used in all of the ^{13}C CP−MAS experiments, which employed a variable-amplitude cross-polarization pulse sequence. A sample rotational speed of 5 kHz was employed in the ^{29}Si

(23) Ikeda, T.; Saha, S.; Aprahamian, I.; Leung, K. C.-F.; Williams, A.; Deng, W.-Q.; Flood, A. H.; Goddard, W. A., III; Stoddart, J. F. *Chem.—Asian J.* **2007**, *2*, 76–93.
(24) (a) Mao, P. C.-M.; Mouscadet, J.-F.; Leh, H.; Auclair, C.; Hsu, L.-Y. *Chem. Pharm. Bull.* **2002**, *50*, 1634–1637. (b) Meng, F.; Hua, J.; Chen, K.; Tian, H.; Zuppiroli, L.; Nüesch, F. *J. Mater. Chem.* **2005**, *15*, 979–986.
(25) Ashton, P. R.; Königer, R.; Stoddart, J. F.; Alker, D.; Harding, V. D. *J. Org. Chem.* **1996**, *61*, 903–908.

CP−MAS experiments, which were performed with a normal cross-polarization pulse sequence. The contact times for ^{13}C and ^{29}Si CP−MAS solid-state NMR spectroscopies were 1.5 and 7.5 ms, respectively. All of the ^{13}C spectra were referenced to the methylene peak of adamantane at +37.77 ppm as a secondary reference for the ^{13}C chemical shift scale with Me_4Si defined as 0 ppm. All of the ^{29}Si spectra were referenced to tetra(trimethylsilyl)silane ($[(Me_3)_3Si]_4Si$) at −9.8 ppm as a secondary reference for the ^{29}Si chemical shift scale with Me_4Si defined as 0 ppm. The Hartman−Hahn match was set by using adamantane and tetra(trimethylsilyl)-silane for ^{13}C and ^{29}Si, respectively, and a typical 90° pulse width was 4 μs. High-resolution matrix-assisted laser desorption/ionization (HR-MALDI) spectra were measured on an AppliedBiosystems DE-STR MALDI time-of-flight mass spectrometer. The reported molecular mass (*m*/*z*) values were from the most abundant monoisotopic mass. The microcalorimetric titrations were performed using an isothermal titration microcalorimeter (MicroCal Inc., model no. VP-ITC) at atmospheric pressure and 25 °C in an aqueous buffer solution. In each run, a buffer solution of the β-CD host in a 0.250 mL syringe was injected sequentially with stirring at 300 rpm into a buffer solution of the guest molecule in the sample cell (1.4 mL volume). A control experiment was performed to determine the heat of dilution by injecting a host buffer solution into a pure buffer solution containing no guest. The dilution enthalpy was subtracted from the apparent enthalpy obtained in each titration run, and the net reaction enthalpy was analyzed using a single-site binding model. The Origin software (MicroCal) was employed to determine simultaneously the complex formation constant (K_f) and the reaction enthalpy (ΔH^0) along with the standard deviation on the basis of the scatter of data points from a single titration experiment. Three independent titration experiments were performed in order to afford self-consistent parameters that gave the averaged values. TEM images were collected on a JEOL JEM1200-EX instrument. Powder XRD patterns were collected using a Philips X'Pert Pro diffractometer equipped with Cu KR radiation. UV−vis spectra were collected using a Cary 5000 UV−vis−NIR spectrophotometer. The controlled release profiles were obtained via luminescence spectroscopy using an Acton SpectraPro 2300i CCD detector and either a Coherent Cube 375-16C laser or a Coherent Cube 445-40C laser.

Diamino-β-CD Derivative 5. Per-6-iodo-β-CD[25] (1.90 g, 1.0 mmol) was dissolved in dry ethylenediamine (5 mL) under an Ar atmosphere. The reaction mixture was stirred at 80 °C for 7 h and then cooled to room temperature, after which the solvent was removed in vacuo. The residue was dissolved in H_2O (15 mL), and the solution was poured into Me_2CO (200 mL). The precipitate that formed in Me_2CO was collected by filtration. The crude product was dissolved in H_2O (10 mL) and subsequently purified on a Sephadex G-25 column with H_2O as the eluent to give compound **5** (1.29 g, 90%) as a colorless solid. ^1H NMR (500 MHz, D_2O, 25 °C, TMS): δ 2.62−2.81 (m, 28H, NCH_2CH_2N), 3.28−3.79 (m, 42H, β-CD-H_{2-6}), 4.98−5.01 (d, 7H, β-CD-H_1). ^{13}C NMR (125 MHz, D_2O, 25 °C, TMS): δ 111.6, 89.1, 74.5, 73.3, 72.2, 52.3, 48.9, 41.4. MS (HR-MALDI) *m*/*z*: Calcd for $C_{56}H_{112}N_{14}O_{28}$, 1428.7770; found, 1427.7594 [M^+].

Plug 7. The procedure is outlined in Scheme 3. A mixture of rhodamine B (0.96 g, 2.0 mmol), the benzidine oligoethylene glycol derivative[23] (1.13 g, 2.1 mmol), DCC (0.62 g, 3.0 mmol), and DMAP (10 mg) in anhydrous *N*,*N*-dimethylformamide (DMF, 50 mL) was stirred for 4 h at room temperature under an Ar atmosphere. The resulting suspension was filtered, and the filtrate was evaporated, after which the residue was subjected to column chromatography (SiO_2/EtOAc) to give compound **7** (1.26 g, 63%). ^1H NMR (500 MHz, D_2O, 25 °C, TMS): δ 1.18−1.22 (m, 12H, rhodamine B-Me), 2.63−2.78 (m, 8H, rhodamine B-CH_2N), 2.98−3.33 (m, 32H, CH_2CH_2), 6.45−6.47 (d, 2H, rhodamine B-H), 6.57−6.59 (d, 2H, benzidine-H_α), 6.89 (s, 1H, rhodamine B-H), 6.97−6.99 (d, 2H, rhodamine B-H), 7.16−7.18 (d, 2H, benzidine-H_β), 7.42 (s, 1H, rhodamine B-H), 7.56−7.58 (m, 2H, rhodamine B-H), 7.85−7.87 (d, 2H, rhodamine B-H). ^{13}C NMR (125 MHz, D_2O, 25 °C, TMS): δ 167.4, 160.3, 155.1, 147.3, 140.3, 138.7, 134.8, 133.5, 131.7, 129.3, 128.2, 121.3, 114.6, 112.8, 110.9, 86.4, 70.2, 64.9, 61.8, 48.0, 46.7, 13.2. MS (HR-MALDI) *m*/*z*: Calcd for $C_{56}H_{73}ClN_4O_{10}$, 996.5015; found, 961.5247 [M − Cl]$^+$.

Phosphonate-Covered Silica Nanoparticles 2. Nanoparticles **2** were prepared using an approach similar to that described in literature.[5a] CTMA (0.50 g, 1.4 mmol) was dissolved in a mixture of distilled H_2O (240 mL) and 2 M NaOH (1.75 mL), and the solution was stirred under an atmosphere of N_2 and heated to 80 °C. TEOS (2.5 mL, 2.33 g, 11.2 mmol) was then added to the solution. After 15 min, TPMP (0.65 mL, 0.81 g, 3.4 mmol) was slowly added to the mixture. After the solution was stirred at 80 °C for 2 h, it was cooled down to room temperature, and the nanoparticles that formed were filtered, washed with MeOH and H_2O, and dried at room temperature overnight. In order to remove the surfactant from the nanopores of the nanoparticles, they were suspended in a mixture of MeOH (50 mL) and concentrated HCl (3 mL), and the solution was heated under reflux for 24 h. The nanoparticles **2** were then filtered and washed thoroughly. The product was dried under vacuum prior to its characterization by solid-state NMR spectroscopy, TEM, and powder XRD. ^{13}C CP−MAS solid-state NMR (300 MHz): δ 65, 22, 9.

Isocyanato-Functionalized Nanoparticles 3. Nanoparticles **3** were prepared using a modification of an approach published in the literature.[6a] Phosphonate-covered silica nanoparticles **2** (100 mg) were suspended in anhydrous PhMe (15 mL), and 3-ICPES (50 μL, 0.05 g, 0.2 mmol) was added to the solution. The reaction mixture was stirred at room temperature under an atmosphere of N_2 overnight. The isocyanato-functionalized nanoparticles **3** were isolated by centrifugation, washed with PhMe and MeOH, and dried under vacuum.

Formyl-Functionalized Nanoparticles 4. Isocyanato-functionalized nanoparticles **3** (50 mg) were suspended in anhydrous PhMe (15 mL), and 4-(2-hydroxyethoxy)benzaldehyde (0.02 g, 0.15 mmol) was then added to the solution. The reaction mixture was stirred under reflux overnight under an atmosphere of N_2. The formyl-functionalized nanoparticles **4** were obtained by centrifugation, washed with PhMe and MeOH, and dried under vacuum.

β-CD-Capped Nanoparticles 6. Formyl-functionalized nanoparticles **4** (50 mg) and anhydrous $MgSO_4$ (0.02 g, 0.2 mmol) were suspended in anhydrous DMF (20 mL), and diamino-β-CD derivative **5** (0.03 g, 0.02 mmol) was then added to the solution. While the solution mixture was being stirred at room temperature under an atmosphere of N_2 for 6 h, $NaBH_4$ (0.01 g, 0.25 mmol) was added to it slowly at 0 °C. After the solution had been stirred for 2 h at 0 °C, the reaction was quenched with H_2O at room temperature. The β-CD-capped nanoparticles **6** were isolated by centrifugation, washed with H_2O, and dried under vacuum. ^{13}C CP−MAS solid-state NMR (300 MHz): δ 165, 130, 104, 84, 73, 50, 45, 22, 9. ^{29}Si CP−MAS solid-state NMR (300 MHz): δ −60, −105.

MSNP-Based Nanopistons 1. β-CD-capped nanoparticles **6** (50 mg) were added to an aqueous buffer solution (pH 7) containing NDAD (10 mL, 1.0 mM). The reaction mixture was stirred and sonicated to maximize the dispersion. The solution was then stirred under an atmosphere of N_2 overnight to allow the NDAD to diffuse into the nanopores of the nanoparticles. Plug **7** (0.02 g, 0.02 mmol) was then added to the reaction mixture. After the solution had been stirred under an atmosphere of N_2 for 4 h, the MSNP-based nanopistons **1** were obtained by centrifugation, washed with aqueous buffer solution, and dried under vacuum. The fresh nanoparticles were used immediately for the laser investigations involving fluorescence spectroscopy and release profiles.

β-CD-Capped Nanoparticles 8. Formyl-functionalized nanoparticles **4** (50 mg) were added to an anhydrous DMF solution containing rhodamine B (10 mL, 1.0 mM). The reaction mixture was stirred and sonicated to maximize the dispersion. The solution was then stirred under an atmosphere of N_2 overnight to allow rhodamine B to diffuse into the nanopores of the nanoparticles. The nanoparticles loaded with rhodamine B were obtained by

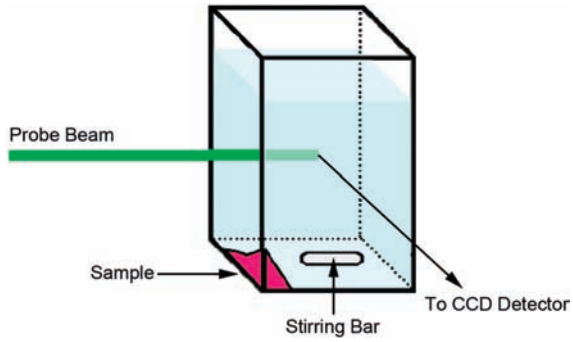

Figure 7. Spectroscopic setup for probing the release from the cargo-loaded nanoparticles. The probe beam was generated from a diode laser. The emission from the solution was collected at an angle of 90° from the probe beam using a N_2-cooled CCD detector.

centrifugation and then added to an anhydrous DMF solution (20 mL) containing anhydrous $MgSO_4$ (0.02 g, 0.2 mmol) under an atmosphere of N_2. Diamino-β-CD derivative **5** (0.03 g, 0.02 mmol) was then added to the solution, and the reaction mixture was stirred at room temperature for 6 h. The capped nanoparticles **8** were isolated by centrifugation, washed with anhydrous DMF, and dried under vacuum. The fresh nanoparticles were used immediately for the laser investigations involving fluorescence spectroscopy and release profiles.

Release Analysis of Nanoparticles. Cargo-loaded nanoparticles were examined using the spectroscopic setup shown in Figure 7. The nanoparticles (5 mg) were placed in the corner of a cuvette. Distilled H_2O (pH ~7, 5 mL) was added to the cuvette in a dropwise fashion in order to prevent the nanoparticles from dispersing into the solution. A 1 mm stirring bar was added to the cuvette. The solution in the cuvette was stirred slowly to avoid perturbing the nanoparticles. The solution was monitored using a CCD detector, which collected the emission spectra of the solution. A laser probe beam directed into the solution ~2 cm above the bottom of the cuvette was used to excite the released cargo molecules. A suitable filter lens was placed in front of the CCD detector to remove the scattered probe beam. The fluorescence spectra of the released cargo molecules were collected at 1 s intervals during the course of the experiment. The fluorescence intensity at the emission maximum of the cargo molecules was plotted as a function of time in order to generate a release profile. Activation of cargo molecule release from the nanoparticles was accomplished by adjusting the pH values of the solution with addition of HCl solution (0.1 M). The percentage of cargo release was calculated using UV−vis absorption spectroscopy, thus enabling quantitative comparison of the release efficiency. The weight percentage (wt %) was calculated as the released quantity of plugs or cargo divided by the total quantity of loaded nanoparticles.

Acknowledgment. The research at the University of California, Los Angeles, was supported by the U.S. National Science Foundation under Grant CHE-0809384 and by the U.S. Department of Defense under Grant HDTRA1-08-1-0041. The research at Northwestern University (NU) was sponsored by the National Center for Nano Technology Research at the King Abdulaziz City for Science and Technology (KACST) in Saudi Arabia. The authors thank Dr. Turki M. Al-Saud and Dr. Soliman H. Alkhowaiter at KACST for their generous support of this program of research at NU.

JA105371U